Development of a High-Speed Swimming Robot With the Capability of Fish-Like Leaping

Di Chen, Zhengxing Wu, Yan Meng, Min Tan, and Junzhi Yu, *Fellow, IEEE*

***Abstract*—Achieving fast and agile swimming still remains extremely challenging for a self-propelled robotic fish due to the constraint of actuator's propulsion capability. In this article, we report an untethered bioinspired robotic fish, which combines a high-frequency oscillation and a compliant passive mechanism to realize fast swimming, high pitch maneuvers, and even the leaping motion. For pursuing the explosive propulsion of the robotic fish, we propose an actuation system with a powerful output and a compact structure. A dynamic model is established and indicates that the compliant joint is able to modulate the power transmitted to a caudal fin to affect its velocity in the return stroke for generating more peak thrust. The design is validated with extensive experimental results. Namely, the robotic fish can surprisingly reach up to a speed of 3.8 body lengths per second (BL/s). Compared to the case with a rigid joint, dramatic improvements, involving a speed of 1.2 BL/s and a swimming distance of 141.2 m (70.6%), have been obtained, which reveal that besides the high-frequency oscillation, the compliant passive mechanism is also of great significance to perform high-speed swimming. Additionally, the robotic fish demonstrates its high pitch maneuvers by performing an agile front flip motion with a radius of 0.4 BL and an average angular velocity of 439°/s. Most importantly, with a simple control strategy, our robotic fish can remarkably leap out of water completely. Results from this study provide significant insights into the innovative designs of next-generation robotic fishes, which require high speed and maneuverability.**

***Index Terms*—Bioinspired robotic fish, compliant joint, dynamic modeling, high-frequency propulsion, high swimming performance.**

Manuscript received 27 September 2021; revised 18 November 2021; accepted 14 December 2021. Date of publication 6 January 2022; date of current version 17 October 2022. Recommended by Technical Editor M. Defoort and Senior Editor W. J. C. Zhang. This work was supported in part by the National Natural Science Foundation of China under Grants 61725305, T2121002, 61633020, 61973303, and 62022090, in part by the Beijing Natural Science Foundation under Grant 4192060, and in part by the Beijing Nova Program under Grant Z201100006820078. *(Corresponding author: Junzhi Yu.)*

Di Chen, Zhengxing Wu, Yan Meng, and Min Tan are with the School of Artificial Intelligence, University of Chinese Academy of Sciences, Beijing 100049, China, and also with the State Key Laboratory of Management and Control for Complex Systems, Institute of Automation, Chinese Academy of Sciences, Beijing 100190, China (e-mail: chendi2018@ia.ac.cn; zhengxing.wu@ia.ac.cn; mengyan2017@ia.ac.cn; min.tan@ia.ac.cn).

Junzhi Yu is with the State Key Laboratory for Turbulence and Complex Systems, Department of Advanced Manufacturing and Robotics, Beijing Innovation Center for Engineering Science and Advanced Technology, College of Engineering, Peking University, Beijing 100871, China and also with the State Key Laboratory of Management and Control for Complex Systems, Institute of Automation, Chinese Academy of Sciences, Beijing 100190, China (e-mail: junzhi.yu@ia.ac.cn).

Color versions of one or more figures in this article are available at https://doi.org/10.1109/TMECH.2021.3136342.

Digital Object Identifier 10.1109/TMECH.2021.3136342

I. Introduction

FISH has been endowed with excellent capabilities in locomotion after millions of years' evolution in nature. Inspired by that, a robotic fish has attracted a great deal of attentions for its great potential in aquatic applications [1], such as disaster rescue, aquatic environment monitoring [2], and biological study [3]. In the past few decades, many engineers and researchers have devoted to the investigations of the robotic fish, including bioinspired mechanical design [4], hydrodynamics mechanism [5], and locomotion control [6]. Encouragingly, a considerable number of robotic fishes with diverse propulsion modes have emerged, and some good effects have been achieved [7], [8]. However, the vast majority of developed robotic fishes are still far inferior to a real fish in propulsive performance, which restricts the adaptability in an unstructured aquatic environment.

From the perspective of bioinspired engineering, the swimming performance, especially swimming speed, is one of the most engrossing and challenging characteristics of fish. Great efforts have been made to create a variety of mechanical structures for emulating the performance of the real fish. Compared to the "multimotor multijoint" structure, which usually possesses the maneuvers easily but suffers the limitation of actuation frequency [9], [10], the "single-motor multijoint" structure is especially designed toward the high-frequency oscillation and utilized for the development of the fast-swimming robotic fish. For example, Clapham and Hu [11] developed iSplash-II with the maximum speed of 11.6 body lengths per second (BL/s) at 20 Hz. Yu *et al.* [12] also designed a single-motor-actuated robotic fish with the maximum speed of about 3.07 BL/s at 9 Hz. For these robotic fishes, the key point of achieving high speed merely lies on the high-frequency oscillation. The compliant mechanism at low-frequency propulsion has been investigated to improve performance in many aspects [13]–[16]. However, the integration design of the high-frequency propulsion and the compliant mechanism is less proposed. Zhu *et al.* [17] combined a passive peduncle joint with lateral keel to design Tunabot, which achieves a speed of 4.0 BL/s at 15 Hz. Recently, Tunabot Flex has also been developed with three body flexibility configurations to improve the swimming performance [18]. By increasing body flexibility, Tunabot Flex gains a speed of

4.6 BL/s at 8.0 Hz. However, except for iSplash-II, all these robotic fishes are tethered; indeed, Tunabot and Tunabot Flex are also negatively buoyant and unable to accomplish swimming motion independently. Because of the limitation of size and weight, the maneuvers are often neglected, especially in pitch motion. In [19], a compact design of pectoral fin was proposed for better swimming. A microrobotic fish was developed with magnetic drivers for a 3-D motion [20]. The compact design is useful to improve the swimming performance.

At present, the dynamic model of the robotic fish with flexible components has been commonly built to predict the propulsive performance [21]–[23]. Nevertheless, these developed dynamic models mainly focus on the performance at low-frequency actuation. For the restriction of actuation performance, the propulsion mechanism of a robotic fish with compliant components and the high-frequency oscillation has not been studied.

The primary objective of this article is to integrate both the high-frequency oscillation and the compliant passive mechanism into the design of an untethered robotic fish to achieve high swimming performance. To this end, we propose a detailed design scheme with the principles of miniaturization and light weight. Especially, an actuation system with high power density is put forward to ensure the untethered swimming with the high-frequency oscillation. Moreover, a compliant joint is utilized to improve the performance, which allows the robotic fish to passively modulate the power transmitted to the caudal fin. A dynamic model is established and, then, validated by performing experiments to analyze the propulsive mechanism of the high-frequency oscillation and the compliant passive joint in performance improvement. With experimental results, the designed compliant joint shows great advantages in speed and efficiency over the case with a rigid joint. Benefitting from the great superiority in untethered swimming speed, the robotic fish also exhibits dramatic pitch maneuvers and leaping motion. The results in this article bring some significant insights into the optimization of the propulsion performance and provide a novel and reliable solution for an innovative design of the untethered robotic fish with high speed and maneuvers.

The rest of this article is organized as follows. Section II presents the mechanical design and the prototype of the robotic fish in detail. The dynamic model derived with the Lagrangian dynamic method is proposed in Section III. Section IV provides extensive experimental results. The dynamic model is also used to analyze the propulsive mechanism in performance improvement. Finally, Section V concludes this article.

II. Mechatronic Design of the Robotic Fish

A. Overview of the Robotic Prototype

For the purpose of realizing high performance in speed, pitch maneuvers, and leaping motion, the principles of miniaturization and light weight are of prime importance in the design of the robotic fish. Thus, we deliberately develop the robotic fish in many aspects. As illustrated in Fig. 1(a), the robotic fish is designed with a well-streamlined body profile for reducing hydrodynamic drags and mainly comprises three parts: a rigid head, a pair of pectoral fins, and a self-propelled body with a caudal fin. The rigid head is 3-D-printed and mainly used to hold actuators and electronic components. Moreover, for measuring the attitudes and submersion depth of the robotic fish in diving and floating motion, an inertial measurement unit (IMU) and a pressure sensor are mounted in the interior and the exterior of the robotic fish, respectively.

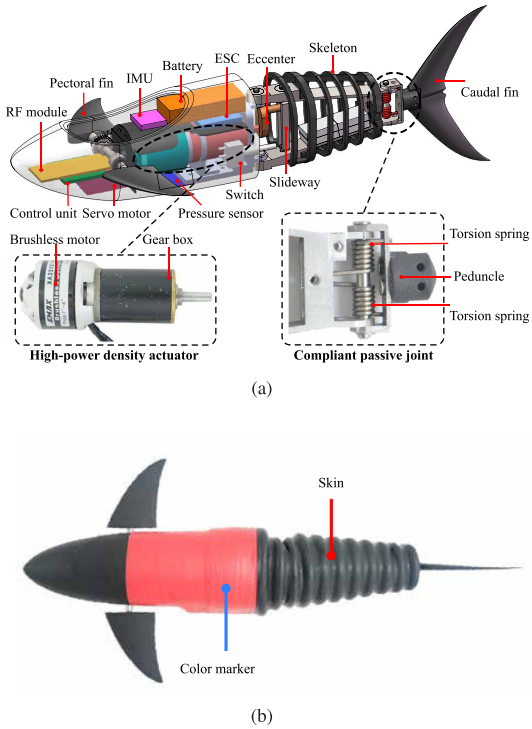

Fig. 1. Overview design of the robotic fish. (a) Side view of the mechanical structure. (b) Top view of the developed prototype.

Because of the space limitation, the pitch mechanism with only one degree of freedom in [24] is used to swim in vertical plane. The pectoral fins (chord: 30 mm, span: 42 mm, and aspect ratio (AR): 2.14) are 3-D-printed with a chordwise cross section of a NACA 0018 airfoil. A compact servo motor actuates the pectoral fins to rotate simultaneously. The "single-motor multijoint" configuration is employed to attain the high-frequency oscillation. More importantly, a high-power-density motor and compliant passive components are integrated together for a high space utilization rate.

According to the system design, the prototype is implemented, as shown in Fig. 1(b). The red marker attaches to the head for detecting the position of the robotic fish. A skin mainly covers the posterior body for waterproof. To reduce the resistance in the rotation of joints, the skins in these locations remain loose. A skeleton is applied to support the skin so as to maintain a streamlined shape with more buoyancy. Finally, the designed robotic fish is 277 mm in length and 380 g in weight. The detailed technical specifications are tabulated in Table I.

B. Design of the Propulsion System

To date, high-speed robotic fishes with the high-frequency oscillation are usually tethered. The size and the weight of the

TABLE I
MAIN TECHNICAL SPECIFICATIONS OF THE ROBOTIC FISH

Items	Characteristics
Dimensions (L × W × H)	∼ 277 mm × 45 mm × 55 mm
Weight	∼ 380 g
Onboard sensors	IMU, Pressure sensor (MS5803)
Power supply	11.1 V 180 mAh Li-ion battery
Actuator	Servo motor×1, Brushless motor×1
Communication unit	Wireless RF (433 MHz)
Control unit	STM32F405RG
Noload maximum frequency	12.95 Hz

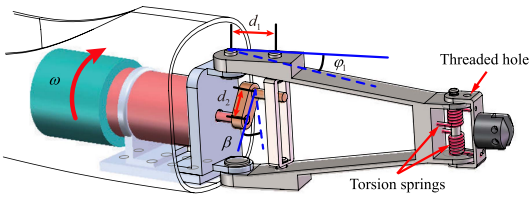

Fig. 2. Illustration of the transmission mechanism with an active joint and a passive joint.

actuator are sacrificed for pursuing a powerful output. Therefore, it is critical to design an actuation system with high power density. As presented in Fig. 1(a), we propose an actuation system with the integration between an outrunner brushless direct current (BLDC) motor (EMAX, XA2212, 980 kV) and a gearbox (Maxon GP 22 C, reduction gear ratio, 14:1). This kind of outrunner BLDC motor is powerful with a compact structure. To overcome the large drag of the fish-like propulsive mechanism in the high-frequency oscillation, we modify the direction of motor's output shaft to connect the gear box for a powerful output with a large torque. With the recorded output power of 147.6 W [25], the actuation system can reach a power density of 1.38 kW/kg.

To realize the high-frequency oscillation, a similar transmission mechanism with fast-swimming robotic fishes is applied, as shown in Fig. 2. An eccenter connects to the output shaft of the gear box, and its drive shaft locates in the slideway. For reducing the friction and avoiding deadlock, the slideway can rotate passively under the action of drive shaft. The power transmission mechanism converts continuous rotation of the motor in one direction into the lateral oscillation of body link so as to produce the fish-like swimming motion, which can improve the actuation efficiency greatly at the high-frequency oscillation. The amplitude of the deflection angle is determined by the offset of the eccenter, which can be adjusted to optimize the performance of propulsion.

As illustrated in Fig. 2, the joint angle can be calculated as follows:

$$\varphi_1 = \arcsin\left(\frac{d_2 \sin(\beta)}{d_1}\right) \tag{1}$$

where d_2 is the offset of the eccenter, $\beta = \omega t$ is the rotation angle of the actuator, ω denotes the angular velocity, and d_1 is the distance between the active joint and the joint of slideway. In this study, we assume that the motor maintains a constant angular velocity during the whole cycle of rotation.

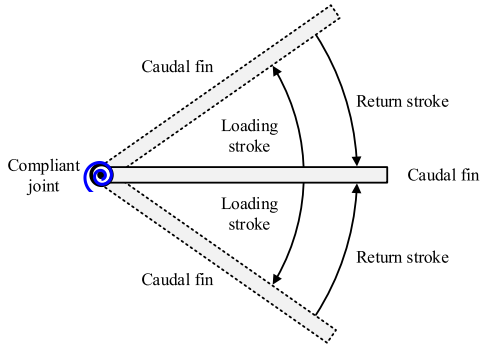

Fig. 3. Illustration of caudal fin's oscillation with a compliant joint.

C. Design of a Compliant Passive Joint

Inspired from the power transmission mechanism of fish, the caudal tendon is simplified as a passive joint with compliant components, which intends to transmit force to the caudal fin effectively. In this study, two identical torsion springs (wire diameter: 1.2 mm, outer diameter: 7.0 mm, and number of active coils: 6) are chosen as the compliant components and installed on the passive joint symmetrically, as shown in Figs. 1(a) and 2. The spring constant of selected torsional springs is 307 g · mm/°. The oscillation of the compliant joint is illustrated in Fig. 3. In the loading stroke, the caudal fin rotates outward to store power as elastic potential energy, during which the hydrodynamic forces as the loading acting on the caudal fin promote the rotation. When torsion springs reach to the maximum deflection, the caudal fin rotates back to return the middle position, during which the torsion springs release the stored energy to promote the motion. In the oscillation of the caudal fin, torsion springs always generate a moment, which attempts to keep the caudal fin in the initial position. The passive joint angle usually lags behind the active joint angle and is affected by many factors.

We also adopt a tuna-inspired caudal fin with a given chordwise cross section of a NACA 0018 airfoil. The maximum width of the fin is 92.3 mm, and the AR is about 6.15. A threaded hole is designed nearby the passive joint, as shown in Fig. 2. By installing a shaft, the passive joint can be locked, and the robotic fish is equipped with a rigid joint. There are no other differences in specifications between the robotic fish with a compliant joint and a rigid joint.

III. DYNAMIC MODELING

In this section, to analyze the mechanism of the compliant joint in performance improvement, the dynamic model with only planar motion is established. Owing to the design of the compliant passive joint, a completely unknown joint angle appears explicitly. Therefore, a Lagrangian dynamic approach is chosen to model the underactuated robot system [26], [27].

A. Kinematic Analysis

In dynamic modeling, the propulsion mechanism of the robotic fish is illustrated in Fig. 4. The inertial coordinate frame is denoted as $O_g - x_g y_g z_g$, and the body coordinate frame is

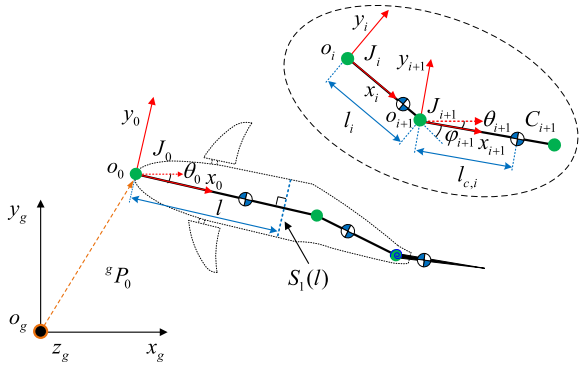

Fig. 4. Schematic illustration of coordinate systems and notations.

defined as $O_i - x_i y_i z_i$. The origin O_0 coincides with the starting point J_0. The x_i-axis is parallel to L_i and directs to joint J_{i+1}. In this article, θ_i $(i = 0, 1, 2)$ represents the angle between link L_i and axis $o_g x_g$. φ_i $(i = 1, 2)$ indicates the angle between the ith link and its prior link, namely, the joint angle of J_i $(i = 1, 2)$. Note that joint J_1 is an active joint and φ_1 is given, and J_2 is a passive joint and φ_2 is unknown. The length of link L_i is denoted as l_i. C_i represents the center of mass (CM) of L_i, and its distance relating to J_i is $l_{c,i}$. The position vector of point in L_i is expressed as $\boldsymbol{r}_i(l)$ in an inertial frame, and l is the distance relating to J_i. $S_i(l)$ is the cross section of L_i with the distance of l. ${}^g\boldsymbol{v}_i$ and ${}^g\boldsymbol{\omega}_i$ denote the translational velocity and angular velocity of L_i with respect to $O_g - x_g y_g z_g$, respectively.

The position vector $\boldsymbol{r}_i(l)$ can be expressed as the vector sum and concisely given in the following form:

$$\boldsymbol{r}_i = {}^gP_0 + {}^gR_0{}^0P_i, \quad (i = 0, 1, 2) \tag{2}$$

where ${}^gP_0$ is the position vector of O_0 in the inertial frame, ${}^gR_0$ indicates the rotation matrix of the coordinate frame $O_0 - x_0 y_0 z_0$ with respect to the inertial frame, and ${}^0P_i$ denotes the position vector of point in L_i in the body frame $O_0 - x_0 y_0 z_0$.

Then, the translational velocity ${}^g\boldsymbol{v}_i$ can be calculated by taking the time derivative of position vector $\boldsymbol{r}_i$

$${}^g\boldsymbol{v}_i = \dot{\boldsymbol{r}}_i = {}^g\dot{R}_0{}^0P_i + {}^gR_0{}^0\dot{P}_i + {}^g\dot{P}_0. \tag{3}$$

In dynamic modeling of planar motion, the angle and angular velocity of L_i in inertial frame can be calculated as follows:

$$\theta_i = \theta_0 + \sum_{j=1}^{i} \varphi_j, \quad (i = 1, 2) \tag{4}$$

$${}^g\omega_i = [0,\ 0,\ \dot{\theta}_i]^T, \quad (i = 0, 1, 2). \tag{5}$$

B. Lagrangian Dynamic Modeling

For the underactuated robot system, some generalized coordinates are selected, and the generalized coordinates vector is given as $\boldsymbol{q} = [x_0, y_0, \theta_0, \theta_2]^T$. The generalized velocities can be expressed as $\dot{\boldsymbol{q}} = [\dot{x}_0, \dot{y}_0, \dot{\theta}_0, \dot{\theta}_2]^T$.

The Lagrangian $L(\boldsymbol{q}, \dot{\boldsymbol{q}})$ expressed as the difference between the kinetic energy and the potential energy of the robot system and the Lagrange equation are given as follows:

$$L(\boldsymbol{q}, \dot{\boldsymbol{q}}) = T(\boldsymbol{q}, \dot{\boldsymbol{q}}) - E(\boldsymbol{q}) \tag{6}$$

$$\frac{d}{dt}\left(\frac{\partial L}{\partial \dot{q}_i}\right) - \left(\frac{\partial L}{\partial q_i}\right) = \tau_i \tag{7}$$

where $T(\boldsymbol{q}, \dot{\boldsymbol{q}})$ and $E(\boldsymbol{q})$ represent the kinetic energy and the potential energy, respectively, and τ_i denotes the generalized force or moment.

For only 2-D motion in the horizontal plane is considered, the total potential energy includes only elastic potential energy of torsion springs. Thus, the Lagrangian function can be presented as follows:

$$L(\boldsymbol{q}, \dot{\boldsymbol{q}}) = \sum_{i=0}^{2} \frac{1}{2} {}^g v_i^T M_i {}^g v_i + \sum_{i=0}^{2} \frac{1}{2} {}^g\omega_i^T I_i {}^g\omega_i - K_s(\varphi_2)^2 \tag{8}$$

where M_i and I_i are the mass matrix and the inertia matrix of the ith link, respectively, involving added mass effects, which are created by accelerating or decelerating the surrounding fluid of the robotic fish, and K_s is the spring constant of the torsion spring. The added mass of link L_i can be calculated by integrating $m_{a,i}(l)$ along the x_i-axis as follows [28]:

$$M_{a,i} = \int_0^{l_i} m_{a,i}(l) dl = \int_0^{l_i} \frac{1}{4} c_{m,i} \rho h_i(l)^2 dl \tag{9}$$

where $c_{m,i}$ is the dimensionless inertia coefficient to describe added mass effects of fluid, $h_i(l)$ indicates the immersed height, and ρ denotes the density of fluid.

C. Hydrodynamic Analysis

In this study, the gravity and buoyancy counteract each other so that the generalized forces are only produced by the hydrodynamic forces. The robotic fish swims freely under the interaction between the robotic fish and the surrounding fluid, which is extremely complicated. For the simplicity of modeling, the fluid where the robotic fish swims is assumed to be inviscid, incompressible, and irrotational. Furthermore, the inertia of rolling and both vertical cross sections are not taken into account in hydrodynamic analysis [29]. The Morrison equation [30] and the lift-drag model [31] are employed to calculate hydrodynamic forces exerted on the body and the caudal fin, respectively.

1) Hydrodynamic Forces on Body: In the Morrison equation method, the hydrodynamic forces mainly include added mass forces and drag forces. The added mass forces are produced by the reaction of the accelerated surrounding fluid and can be derived by multiplying added mass $m_{a,i}$ by the absolute acceleration $\ddot{\boldsymbol{r}}_i(l)$ in inertial frame directly [21]

$$f_{a,i}(l) = -m_{a,i}(l) \ddot{\boldsymbol{r}}_i(l) \tag{10}$$

where $f_{a,i}(l)$ refers to the added mass force exerted on the per unit length of body, and the unit is Newton per meter. By integrating $f_{a,i}(l)$ along the x_i-axis, the added mass force (unit: Newton) acting on the entire body segment can be derived.

The drag force comes from the pressure difference and friction viscosity and is formalized as follows [28]:

$$ {}^{i}f_{d,i}(l) = -\frac{1}{2}\begin{bmatrix} c_{f,i}\rho p_i(l)\,|v_{x,i}(l)|\,v_{x,i}(l) \\ c_{d,i}\rho h_i(l)\,|v_{y,i}(l)|\,v_{y,i}(l) \\ 0 \end{bmatrix} \tag{11} $$

where ${}^{i}f_{d,i}(l)$ indicates the drag force exerted on the per unit length of body, $c_{f,i}$ and $c_{d,i}$ are the dimensionless friction coefficient and drag coefficient to denote the damping effects of fluid, respectively, $p_i(l)$ means the perimeter of the cross section $S_i(l)$, and $v_{x,i}(l)$ and $v_{y,i}(l)$ are the translational velocities in frame $O_i - x_i y_i z_i$.

The hydrodynamic force F_i acting on the entire body link L_i in the inertial frame $O_g - x_g y_g z_g$ can be obtained as follows:

$$ F_i = F_{a,i} + F_{d,i} = \int_0^{l_i} (f_{a,i}(l) + f_{d,i}(l))dl \tag{12} $$

where $F_{a,i}$ and $F_{d,i}$ are the added mass force and the drag force acting on the entire link L_i, respectively. $f_{d,i}(l) = {}^{g}R_i\,{}^{i}f_{d,i}(l)$ means the drag force exerted on the per unit length in the inertial frame.

The moment $M_{i,j}$, which is generated by the hydrodynamic forces F_i acted on joint J_j, can be calculated as follows:

$$ M_{i,j} = \int_0^{l_i} (r_i(l) - r(J_j)) \times (f_{a,i}(l) + f_{d,i}(l))dl \tag{13} $$

where $i = 1, 2$, $j = 0, 2$, and $r(J_j)$ indicates the position vector of joint J_i in the inertial frame.

2) Hydrodynamic Forces on the Caudal Fin: In the development of the robotic fish, we select a lunate caudal fin with an airfoil profile to achieve underwater propulsion. For evaluating its hydrodynamic forces, the lift force and the drag force are calculated as follows [29]:

$$ \begin{cases} F_L = \dfrac{1}{2}\rho C_L(\alpha) v_2^2 A_2 \\ F_D = \dfrac{1}{2}\rho C_D(\alpha) v_2^2 A_2 \end{cases} \tag{14} $$

where $C_L(\alpha)$ and $C_D(\alpha)$ are the dimensionless lift coefficient and drag coefficient, respectively, which are dependent on the angle of attack α, v_2 is the linear velocity magnitude of the caudal fin, and A_2 denotes the wetted area of the caudal fin.

According to the hydrodynamic analysis, the generalized forces and moments are obtained as follows:

$$ \begin{cases} F_x = \sum_{i=0}^{2} F_{i,x} \\ F_y = \sum_{i=0}^{2} F_{i,y} \\ \tau_0 = \sum_{i=0}^{1} M_{i,0,z} + \tau_{2,0,z} \\ \tau_2 = \sum_{i=0}^{1} M_{i,2,z} + \tau_{2,2,z} \end{cases} \tag{15} $$

where $F_{i,x}$ and $F_{i,y}$ denote the components of F_i in the direction of the x_g-axis and the y_g-axis, respectively, $M_{i,0,z}$ and $\tau_{2,0,z}$ are the moments produced by hydrodynamic forces acting on link L_i and the caudal fin applied to joint J_0 in the z_g-axis, respectively, and $M_{i,2,z}$ and $\tau_{2,2,z}$ are the moments produced by hydrodynamic forces acting on link L_i and the caudal fin exerted on joint J_2 in the z_g-axis, respectively.

TABLE II
PHYSICAL PARAMETERS USED FOR THE DYNAMIC MODEL

Item	Unit	L_0	L_1	L_2
m_i	kg	0.263	0.105	0.012
l_i	m	0.143	0.075	0.059
$l_{c,i}$	m	0.094	0.034	0.012
$I_{r,i}$	kg·m^2 ($\times 10^{-4}$)	25.8	1.93	0.039
A_i	m^2 ($\times 10^{-4}$)	-	-	13.84

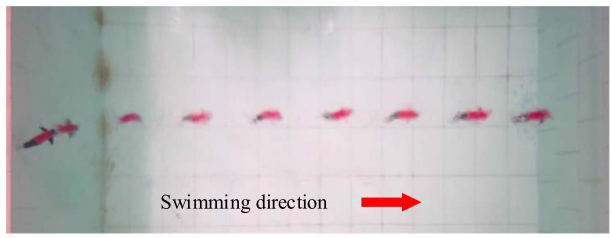

Fig. 5. Overlaid image of straightforward swimming at a tail-beating frequency of 12.82 Hz (time interval is 0.4 s).

Finally, by instituting equations of (15) into (7), the robotic fish system is described completely. With appropriate parameters, we can take advantage of these equations to estimate the locomotion states of the robotic fish.

IV. EXPERIMENTS AND ANALYSES

In the interest of exploring the swimming performance and validating the presented dynamic model, extensive experiments are carried out in this section. A little positive buoyancy (ratio of added balance weight for neutral buoyancy to the weight of the robotic fish η, 15:380) is kept to enhance the stability since the robotic fish is sensitive to disturbances during the fast-swimming motion. Systematic tests on the propulsion performance have been conducted in a water tank with the size of 5 m × 4 m × 1.2 m. A global vision camera is installed on the top of the tank to record the swimming motion, and a specific developed motion measurement system is applied to analyze the swimming speed [32]. In the experiments, the position of the global camera is fixed, and the height between the global camera and the water surface remains constant. GoPro cameras are used to capture the pitching motion and the leaping motion for exhibiting the impressive capabilities intuitively.

A. Free-Swimming Testing and Dynamic Model Validation

In the dynamic model, numerous parameters, including physical parameters and hydrodynamic parameters, are contained. We can easily acquire these physical parameters from the mechanical model of the designed robotic fish in SolidWorks, as tabulated in Table II. Fig. 5 shows the overlaid image of the straightforward swimming motion with the maximum tail-beating frequency of 12.82 Hz. The corresponding speed curve is shown in Fig. 6(a). The maximum instantaneous speed reaches up to 1.19 m/s (4.3 BL/s). The steady speed is defined as the average speed of last two-fifths time interval, where the swimming motion

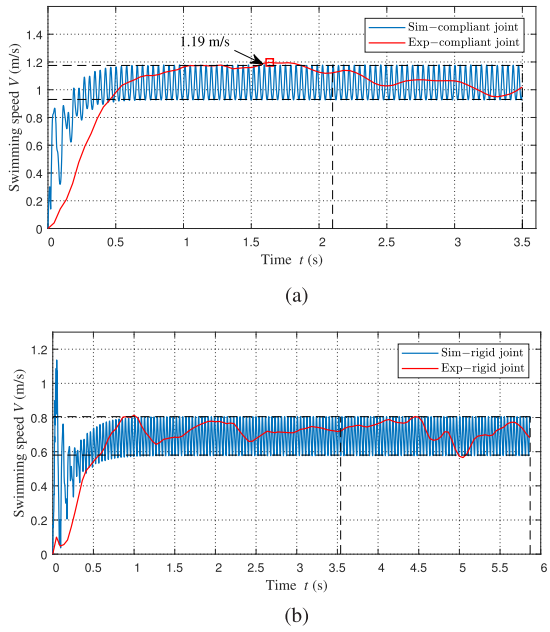

Fig. 6. Comparisons between the experimental speed and the simulated speed. (a) Comparison for the robotic fish with a compliant joint at 12.82 Hz. (b) Comparison for the robotic fish with a rigid joint at 12.77 Hz.

TABLE III
HYDRODYNAMIC PARAMETERS OF THE IDENTIFIED DYNAMIC MODEL

Parameters	$c_{m,0}$	$c_{m,1}$	$c_{f,0}$	$c_{f,1}$	$c_{d,0}$	$c_{d,1}$
Value	0.16	0.11	0.11	0.055	2.3	2.0

trends to become stable. It achieves a steady speed of 1.05 m/s (3.8 BL/s). In addition, experiments of the robotic fish with a rigid joint were also conducted, and the curve at the maximum frequency of 12.77 Hz is presented in Fig. 6(b). The steady swimming speed reaches 0.73 m/s (2.6 BL/s). In this article, we mainly concentrate on the swimming speed of the robotic fish; therefore, two speed curves with maximum frequencies are chosen to identify hydrodynamic parameters. We tuned these parameters manually to fit the simulation speeds with experimental speeds. The comparisons are shown in Fig. 6. For the restriction of global camera's frame rate, the curves of experimental data are much smoother than the simulated results. It should be noted that in the dynamic model, the rigid joint is approximated as a joint with large enough stiffness. Finally, the hydrodynamic parameters are tabulated in Table III.

For evaluating the proposed dynamic model with identified hydrodynamic parameters, the steady speeds of both the simulation and the experiment are compared. As shown in Fig. 7, the steady speeds all present a linear relation with the tail-beating frequency, and the simulated results match well with experimental results. With the increase in frequency, the steady speeds of the robotic fish with a rigid joint are much lower than that of the robotic fish with a compliant joint, and the maximum improvement in speed can achieve 1.2 BL/s, which suggests that the compliant components play a significant role in enhancing the swimming speed under the high-frequency oscillation.

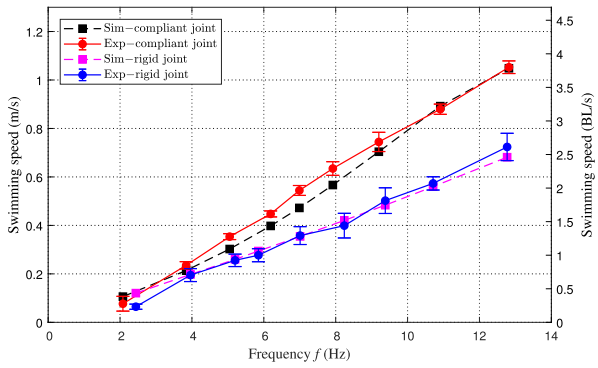

Fig. 7. Comparisons between experiment measurement and model prediction of steady speed for the robotic fish at different tail-beating frequencies.

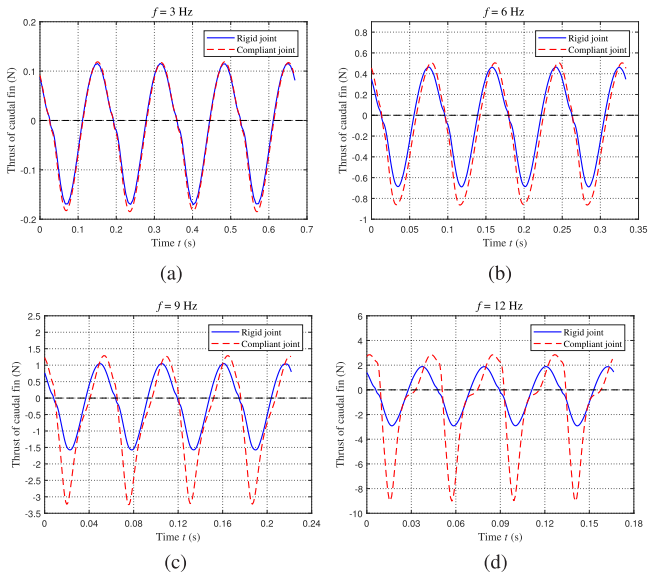

Fig. 8. Comparisons of caudal fin's thrust between the robotic fish with a compliant joint and a rigid joint at different oscillation frequencies. (a) $f = 3$ Hz. (b) $f = 6$ Hz. (c) $f = 9$ Hz. (d) $f = 12$ Hz.

B. Model Analysis for Performance Improvement

As presented in experiments, our robotic fish with a compliant joint shows clear speed merit over the case with a rigid joint. With the validated dynamic model, the state variables are acquired, and the thrust of the caudal fin in the swimming direction can be estimated as

$$F_{\text{thrust}}(t) = F_{2,x}(t)\cos(\theta_0) + F_{2,y}(t)\sin(\theta_0). \tag{16}$$

As an illustrative example, we present the thrust curves under four frequencies intuitively. As shown in Fig. 8, at the frequency of 3 Hz, the curves almost coincide with each other, which is due to the less deflection angle of torsion springs at low frequency. However, along with the increase in frequency, even the drag with the compliant joint raises slightly, the peak value of thrust with the compliant joint increases more apparently than the case with the rigid joint.

With a symmetric actuation pattern of the torsional spring, the total elastic potential energy during one cycle of oscillation is

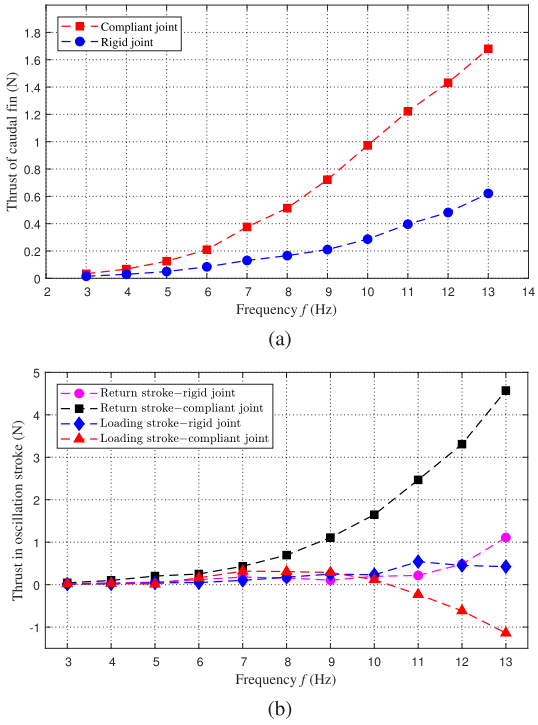

Fig. 9. Comparisons of caudal fin's average thrust. (a) Average thrust in one oscillation cycle. (b) Average thrust in loading and return strokes.

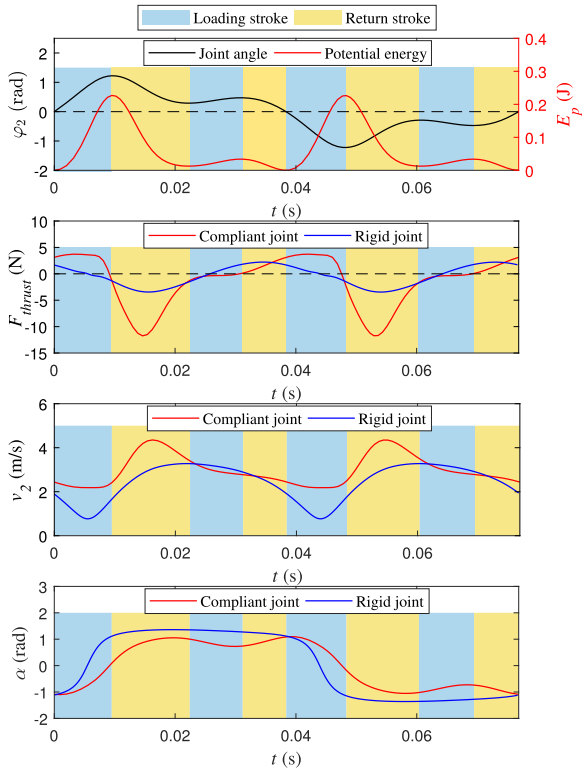

Fig. 10. State variables in one period of the caudal fin oscillation at the frequency of 13 Hz.

equal to zero, which means that the compliant components only play a role in modulating the power transmitted to the caudal fin without causing any energy loss. To further analyze the role of the compliant joint in performance improvement, we also calculate the average thrust of the caudal fin as follows:

$$\bar{F}^{t}_{\text{thrust}} = \frac{1}{t}\int_{t_0}^{t_0+t} F_{\text{thrust}}(t)dt, (t = T, t_{\text{lo}}, \text{ and } t_{\text{re}}) \qquad (17)$$

where t is the length of time, t_0 is the starting time of a fin-beat cycle, T indicates the period, and t_{lo} and t_{re} denote the duration of loading and return strokes, respectively.

As shown in Fig. 9(a), the average thrust of the caudal fin with both joints increases with frequency, namely, the high-frequency oscillation is an effective way to improve the swimming speed. In addition, the average thrust of the caudal fin with a compliant joint increases more rapidly than that of the caudal fin with a rigid joint, which results in significant speed improvement at high frequency. Fig. 9(b) presents the thrust of the caudal fin in each stroke. With regard to the caudal fin with a rigid joint, for the less effects of compliant components, the thrust does not vary obviously. As for the caudal fin with a compliant joint, when the frequency is less than 10 Hz, the average thrust in the loading stroke does not change much. However, when the frequency exceeds 10 Hz, the average thrust starts becoming drag and increases with the frequency rapidly. At the same time, the thrust in the return stroke increases more apparently with the increase of frequency. That is to say, for the caudal fin with a compliant joint, the significant increase in the thrust is mainly attributed to the obvious increase in the return stroke.

The thrust is determined by many state variables, such as angle of attack, velocity, yaw angle, and so on, which makes it difficult to analyze the effect of the compliant joint exactly. Among these variables, the angle of attack α and the velocity v_2 are mainly concerned. As illustrated in Fig. 10, we give the state variables in one cycle at 13 Hz to analyze their varieties in each stroke. It is interesting to note that before achieving the end of the return stroke, the caudal fin rotates outward slightly, bringing a reappearance of the loading stroke. The comparisons involving thrust F_{thrust}, velocity v_2, and angle of attack α are given. In the main loading stroke, for the caudal fin with a compliant joint, even higher speed is obtained, the discrepancy of α leads to producing more drags than the case with a rigid joint. In another loading stroke, the thrust changes slightly, which indicates that the appearance of this loading stroke affects the propulsion less.

From Fig. 10, we can find that the increase in the thrust mainly occurs in the return stroke, where torsion springs release the stored energy and generate a moment to promote the caudal fin oscillating back to the middle position. Before increasing the peak value of the thrust, the amplitude of v_2 increases distinctly, and the angle of attack α determined by the direction of velocity also increases rapidly to approach to that of the case with a rigid joint. In this phase, both the variations of v_2 and α result in the increase in the thrust. After this, the angle of attack α changes slightly, and the rapid decrease in v_2 primarily causes the drop in the thrust. Therefore, the power modulation of the compliant joint is mostly to affect caudal fin's velocity including the direction and the amplitude in the return stroke to produce

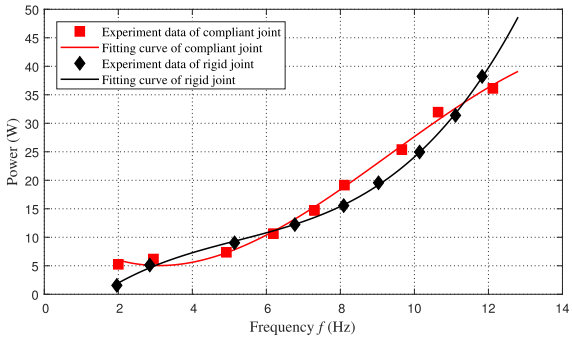

Fig. 11. Average power and fitting curves versus the tail-beating frequency.

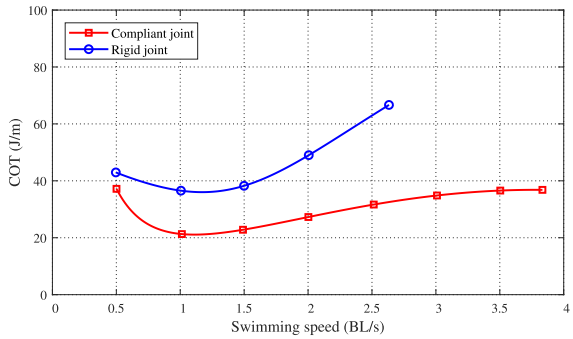

Fig. 12. Comparison of COT versus swimming speed given in body lengths per second.

more peak thrust. From a flow field point of view, during the return stoke, the caudal fin with a compliant joint gains a higher speed to oscillate to the middle position, resulting in a more powerful jet flow to produce larger thrust.

As mentioned above, we can draw some conclusions to better understand why the developed robotic fish can reach a fast swimming motion.

1) The thrust can be effectively improved by increasing the frequency of oscillation.
2) Relating to the rigid joint, the compliant joint helps to obtain a larger thrust when oscillating at high frequency.
3) As for the caudal fin with a compliant joint, the significant increase in the thrust mainly occurs in the return stroke of oscillation.
4) The compliant joint plays a role of the power modulation to affect caudal fin's velocity in the return stroke to produce more peak thrust.

C. Power Measurement

In the experiments, a current transducer and a voltage sensor were adopted to measure both signals. A data acquisition device was used to record the signals synchronously with the sampling rate of 300 Hz in at least 6 s. Both voltage and current signal data were processed with a moving average filter to calculate the average power. For the constraints of space and interference of magnetic field, in the experiments of power measurement, a tethered situation has to be selected. Namely, measurement modules were put outside of the robotic fish to measure signals. The power of the robotic fish with a compliant joint and a rigid joint was measured to analyze the effect of the designed compliant joint. As shown in Fig. 11, the consumed power increases with the increase in the tail-beating frequency. The maximum power of the robotic fish with a compliant joint and a rigid joint is 36.1 W (12.1 Hz) and 38.2 W (11.8 Hz), respectively.

The cost of transport (COT) defined as the ratio of the consumed power to the swimming speed is calculated to analyze the propulsive efficiency, which denotes the consumed energy per unit distance traveled [17]

$$\mathrm{COT} = \frac{P}{V} \tag{18}$$

where P is the output power of the battery.

With respect to the measurements of speed and power, some differences in the maximum tail-beating frequencies have emerged, which is mainly attributed to the existence of a cable. Therefore, the polynomial fitting method is adopted to describe the relationship between power and frequency, as shown in Fig. 11. The relationship between speed and frequency is also fitted. In this way, we can obtain the power and the speed at the same frequency, and then, the COT is calculated, as shown in Fig. 12. The COT of the robotic fish with a compliant joint is much lower than that of the robotic fish with a rigid joint. That is to say, the designed compliant joint not only endows the robotic fish with high speed, but also enhances its efficiency. At the speed of 1.1 BL/s, the robotic fish with a compliant joint reaches its lowest COT of 21.1 J/m. The minimum COT of the robotic fish with a rigid joint is about 36.0 J/m with the speed of 1.2 BL/s. With respect to the equipped 2-Wh battery, theoretically, the designed robotic fish can swim a longest distance of 341.2 m, which increases about 141.2 m (70.6%) relating to that of the robotic fish with a rigid joint. It should be noted that the tethered measurement causes more power.

D. Pitch Maneuvers

One of the main foci of our robotic fish is to achieve high maneuvers in the vertical plane. During the swimming motion, by adjusting the deflection angle, the pectoral fins can produce pitch moments to realize the descending and ascending motions. Specifically, our robotic fish is able to perform flipping swimming motion agilely with a given deflection angle of pectoral fins and powerful propulsion of the caudal fin. For our robotic fish, the center of buoyancy is very close to the CM, which generates a very small moment. Therefore, the effects of buoyancy on pitch maneuvers can be neglected. Fig. 13 displays the snapshot sequence of the robotic fish executing a front flip motion. A yellow circle line is used to approximate the trajectory of the front flip motion. The radius of the front flip is only about 11 cm (0.4 BL). The period of 360° front flip motion is about 0.82 s. In other words, the average angular velocity can amazingly reach up to 439°/s. Compared with other robotic fishes, such as Yu's robotic dolphin (360° front flip, 6.52 s) [33] and Zhang's robotic fish (180° back flip, 4.4 s) [34], our robotic fish is largely superior in angular velocity.

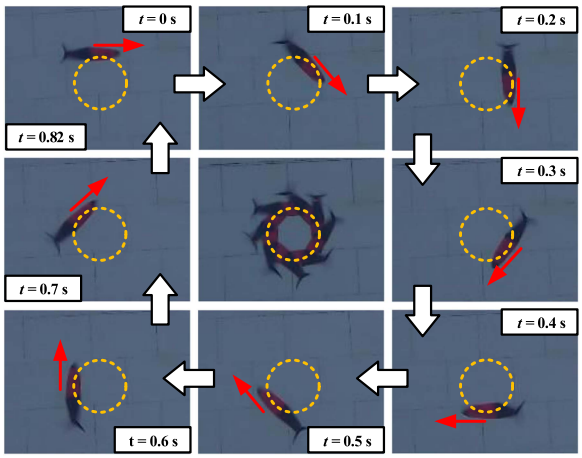

Fig. 13. Snapshot sequence of the robotic fish with a front flip swimming motion; the rotation angle of pectoral fins is -30°.

E. Leaping Motion Tests

In nature, many aquatic animals, such as dolphin, flying fish, and piraputanga, can effortlessly leap out of water in a split-second. However, it is very difficult for a robotic fish to realize the leaping motion. Along with high-speed swimming, it is exceedingly challenging to leap out of water with locomotion control. Therefore, we explored the possibility of autonomous leaping motion with a simple control strategy. It is worth noting that to further prove the capability of the leaping motion, the ratio η is adjusted from 15:380 to 5:390 by adding extra balance weight. Thus, the effect of positive buoyancy on increasing swimming speed is very limited. As shown in Fig. 14(a), phases I–III represent the straightforward swimming motion, the diving motion, and the floating motion, respectively. The proportional–integral–derivative algorithms are utilized to make the robotic fish reach an empirically given depth (0.45 m) with a range of pitch angles from 40° to 60°, and then, the robotic fish accelerates abruptly with the maximum oscillation frequency to increase the existing speed, which is corresponding to phase IV. With the changes of depth, the slight changes of buoyancy bring some disturbances to locomotion control. As shown in Fig. 14(b), a nearly vertical leap is achieved completely in phase V, which requires higher swimming speed owing to the lifting height of the CM. Finally, the robotic fish drops into water.

The measured pitch angle and depth are shown in Fig. 15. Our robotic fish accelerates from the depth of 0.45 m with a pitch angle of 44°. As a result of head's high-frequency oscillation in air, the accurate data are unavailable. Therefore, the testing data of depth are set to zero when the robotic fish escapes from the water surface. To the best of authors' knowledge, besides the robotic dolphin [7] that achieves the successful leaping motion by superb posture adjustment, our robotic fish is the only one that realizes the nearly vertical fish-like leaping with high swimming speed. The aerial phase that starts from piercing water surface to reentering water completely lasts about 0.54 s, which is shorter than the time of the robotic dolphin in [7].

In the water-exit process, our robotic fish still oscillates to produce thrust to assist the leaping motion, and no posture

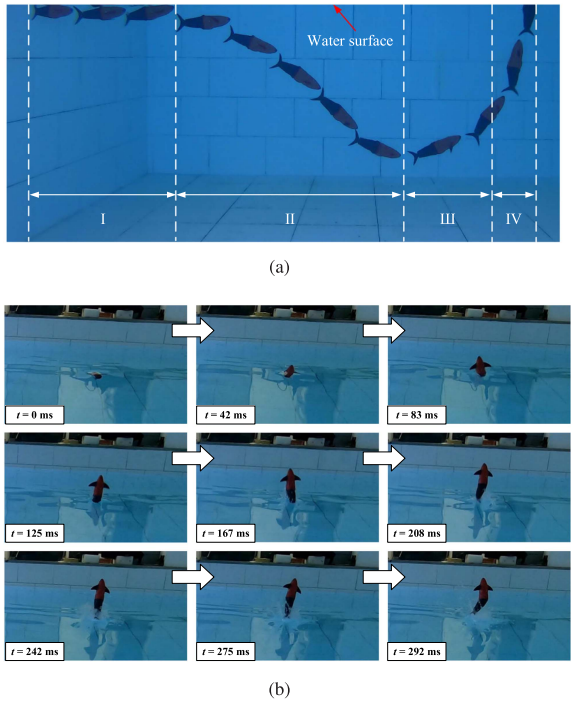

Fig. 14. Snapshot sequence of a successful leaping motion. (a) Overlaid image of swimming pathway in underwater. (b) Leaping image sequence.

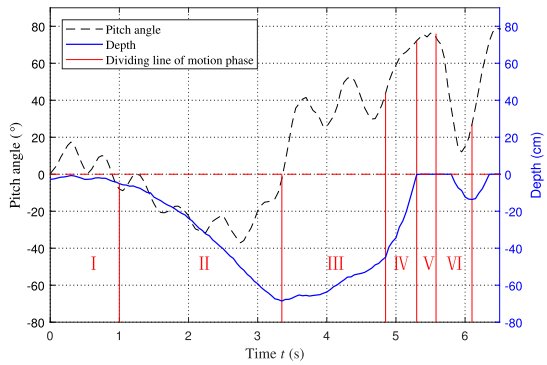

Fig. 15. Plots of pitch angle and submersion depth versus time in the leaping motion.

adjustment is conducted. At the beginning, because the drag force decreases suddenly, the speed may increase slightly. However, with the increase in the leaping height, the buoyant force decreases gradually. The gravity becomes the dominant force, and the downward acceleration trends to increase. When the oscillated posterior body emerges from water, some water is also carried into air. Furthermore, when the caudal fin crosses the water surface, the thrust decreases rapidly, and large quantities of sprays are splashed. All these factors cause a gradually increased and downward acceleration, making a clear drop in speed. When leaping out of water completely, the robotic fish follows a ballistic trajectory under the action of gravity. For the limited speed, this phase is momentary. By increasing swimming speed and exploring the mechanism with less speed loss, the leaping performance can be improved significantly.

TABLE IV
COMPARISON WITH EXISTING ROBOTIC FISHES

Items	Robotic dolphin [7]	iSplash-II [11]	Robotic fish [12]	Tunabot [17]	Tunabot Flex [18]	Our robotic fish
Weight (g)	4700	835	863	306	190	380
Power density (kW/kg)	0.46	-	-	0.53	0.53	1.38
Maximum speed (BL/s)	2.85	11.6	3.07	4.0	4.6	3.8
Frequency (Hz)	4.65	20	9	15	8	12.82
Free swimming	Yes	Yes	No	No	No	Yes
Maneuvers	3D motion	No	Turning motion	No	No	Pitching motion

[1]Note: Parts of data are estimated with the information offered by authors. "–" indicates that the information is not available.

F. Discussion

In this article, we have developed an excellent robotic fish by integrating the high-frequency oscillation and the compliant joint. As tabulated in Table IV, we compare our robotic fish with some robotic fishes, which are competitive in swimming speed. As regards the swimming performance, the robotic dolphin [7] can realize 3-D swimming, and the robotic fish [12] can achieve both the straight swimming motion and the turning motion. However, for the limitation of actuation frequency, their swimming speeds are slower than the speed of our robotic fish distinctly. iSplash-II, Tunabot, and Tunabot Flex outperform our robotic fish in the swimming speed. However, the gap between Tunabot and our robotic fish is narrowed. It is worth noting that not only maneuver motion, but also independent swimming motion is unavailable for both Tunabot and Tunabot Flex. Additionally, although the speed of our robotic fish is lower than that of three robots, our robotic fish is largely superior to all the other robots in pitch maneuvers. More interestingly, benefitting from the great superiority in untethered swimming speed and pitching maneuvers, our robotic fish can leap out of water completely, which exhibits its extraordinary locomotion performance. The leaping motion of a large-size robotic dolphin [7] mainly relies on the excellent posture control to allow its body to separate from water completely. Our robotic fish possesses higher swimming speed, and the characteristics of miniaturization and lightweight are better suitable for the locomotion of the cross domain. By equipping a pair of foldable pectoral fins, our robotic fish has a great potential to evolve into an aquatic–aerial unmanned vehicle (just like flying fish) to implement tasks in water and air. The results have demonstrated that our robotic fish is outstanding in the swimming performance.

While the designed robotic fish holds the promising swimming performance, the efficiency of our robotic fish is much lower than that of Tunabot [17] and Tunabot Flex [18]. We mainly attribute such a phenomenon to head's high-frequency oscillation, which produces drags apparently. Sprays also cause the considerable dissipation of energy. The efficiency is not a major consideration for the first prototype. In this article, we mainly focus on the efficiency improvement, and the results have verified its effectiveness.

V. CONCLUSION

In this article, we developed a novel untethered robotic fish with the capability of remarkable swimming speed, high pitch maneuvers, and even leaping motion. Following the principles of miniaturization and light weight, we presented two critical specifics. First, we proposed an actuator system with high power density, which ensures the fast untethered swimming under the constraints of size and weight. Second, inspired by the power transmission mechanism of the caudal tendon, a compliant passive joint was also designed to improve the swimming performance. We also built a dynamic model to explore the propulsive mechanism under the integration of the high-frequency oscillation and the compliant joint, and the analyses suggested that at the high-frequency oscillation, the compliant joint can modulate the power transmitted to the caudal fin to generate more peak thrust in the return stroke. Extensive experimental results exhibited the impressive performance. Meanwhile, the compliant joint showed clear advantages over the rigid joint in speed and efficiency. More attractively, an autonomous leaping motion was performed to show its tremendous potentiality in designing an aquatic–aerial unmanned vehicle. Comparisons with the existing robotic fishes were demonstrated the superiority of our robotic fish in untethered swimming speed, pitch maneuvers, and light weight with small size. In brief, this study provides a useful guidance for designing a robotic fish with high performance and allows us to pursue a more comprehensive understanding of biomechanics in high-speed swimming.

In future work, we will endeavor to improve the propulsion performance through mechanical design optimization. A pair of foldable pectoral fins will also be considered to realize gliding motion in air.

REFERENCES

[1] J. Yu, L. Wen, and Z. Ren, "A survey on fabrication, control, and hydrodynamic function of biomimetic robotic fish," *Sci. China Technol. Sci.*, vol. 60, no. 9, pp. 1365–1380, 2017.
[2] Z. Wu, J. Liu, J. Yu, and H. Fang, "Development of a novel robotic dolphin and its application to water quality monitoring," *IEEE/ASME Trans. Mechatronics*, vol. 22, no. 5, pp. 2130–2140, Oct. 2017.
[3] S. Marras and M. Porfiri, "Fish and robots swimming together: Attraction towards the robot demands biomimetic locomotion," *J. Roy. Soc. Interface*, vol. 9, no. 73, pp. 1856–1868, 2012.
[4] A. Raj and A. Thakur, "Fish-inspired robots: Design, sensing, actuation, and autonomy—A review of research," *Bioinspiration Biomimetics*, vol. 11, no. 3, 2016, Art. no. 031001.
[5] Z. Ren, X. Yang, T. Wang, and L. Wen, "Hydrodynamics of a robotic fish tail: Effects of the caudal peduncle, fin ray motions and the flow speed," *Bioinspiration Biomimetics*, vol. 11, no. 1, 2016, Art. no. 016008.
[6] J. Yu, Z. Wu, Z. Su, T. Wang, and S. Qi, "Motion control strategies for a repetitive leaping robotic dolphin," *IEEE/ASME Trans. Mechatronics*, vol. 24, no. 3, pp. 913–923, Jun. 2019.
[7] J. Yu, Z. Su, Z. Wu, and M. Tan, "Development of a fast-swimming dolphin robot capable of leaping," *IEEE/ASME Trans. Mechatronics*, vol. 21, no. 5, pp. 2307–2316, Oct. 2016.
[8] R. K. Katzschmann, J. DelPreto, R. MacCurdy, and D. Rus, "Exploration of underwater life with an acoustically controlled soft robotic fish," *Sci. Robot.*, vol. 3, no. 16, 2018, Art. no. eaar3449.

[9] J. Liu and H. Hu, "Biological inspiration: From carangiform fish to multi-joint robotic fish," *J. Bionic Eng.*, vol. 7, no. 1, pp. 35–48, 2010.
[10] Z. Su, J. Yu, M. Tan, and J. Zhang, "Implementing flexible and fast turning maneuvers of a multijoint robotic fish," *IEEE/ASME Trans. Mechatronics*, vol. 19, no. 1, pp. 329–338, Feb. 2014.
[11] R. J. Clapham and H. Hu, "iSplash-II: Realizing fast carangiform swimming to outperform a real fish," in *Proc. IEEE Int. Conf. Intell. Rob. Syst.*, Chicago, IL, USA, 2014, pp. 1080–1086.
[12] J. Yu, C. Zhang, and L. Liu, "Design and control of a single-motor-actuated robotic fish capable of fast swimming and maneuverability," *IEEE/ASME Trans. Mechatronics*, vol. 21, no. 3, pp. 1711–1719, Jun. 2016.
[13] P. R. Ouyang, R. C. Tjiptoprodjo, W. J. Zhang, and G. S. Yang, "Micro-motion devices technology: The state of arts review," *Int. J. Adv. Manuf. Technol.*, vol. 38, pp. 463–478, 2008.
[14] A. Chen, R. Yin, L. Cao, C. Yuan, H. K. Ding, and W. J. Zhang, "Soft robotics: Definition and research issues," in *Proc. Int. Conf. Mechatronics Mach. Vis. Pract.*, Auckland, New Zealand, 2017, pp. 366–370.
[15] F. Iida and C. Laschi, "Soft robotics: Challenges and perspectives," *Procedia Comput. Sci.*, vol. 7, pp. 99–102, 2011.
[16] P. R. Ouyang, W. J. Zhang, and M. M. Gupta, "A new compliant mechanical amplifier based on a symmetric five-bar topology," *J. Mech. Des.*, vol. 130, no. 10, 2008, Art. no. 104501.
[17] J. Zhu, C. H. White, D. K. Wainwright, V. Di Santo, G. V. Lauder, and H. Bart-Smith, "Tuna robotics: A high-frequency experimental platform exploring the performance space of swimming fishes," *Sci. Robot.*, vol. 4, no. 34, 2019, Art. no. eaax4615.
[18] C. H. White, G. V. Lauder, and H. Bart-Smith, "Tunabot Flex: A tuna-inspired robot with body flexibility improves high-performance swimming," *Bioinspiration Biomimetics*, vol. 16, no. 2, 2021, Art. no. 026019.
[19] M. Sharifzadeh, Y. Jiang, A. S. Lafmejani, K. Nichols, and D. Auke, "Maneuverable gait selection for a novel fish-inspired robot using a CMAES-assisted workflow," *Bioinspiration Biomimetics*, vol. 16, no. 5, 2021, Art. no. 056017.
[20] Z. Qian, H. Liu, and Z. Bi, "Design and testing of a biomimetic fish robot with rapid prototyping," *Int. J. Syst. Appl. Eng. Develop.*, vol. 9, pp. 159–166, 2015.
[21] V. Kopman, J. Laut, F. Acquaviva, A. Rizzo, and M. Porfiri, "Dynamic modeling of a robotic fish propelled by a compliant tail," *IEEE J. Ocean. Eng.*, vol. 40, no. 1, pp. 209–221, Jan. 2015.
[22] S. B. Behbahani and X. Tan, "Design and modeling of flexible passive rowing joint for robotic fish pectoral fins," *IEEE Trans. Robot.*, vol. 32, no. 5, pp. 1119–1132, Oct. 2016.
[23] D. Chen, Z. Wu, H. Dong, M. Tan, and J. Yu, "Exploration of swimming performance for a biomimetic multi-joint robotic fish with a compliant passive joint," *Bioinspiration Biomimetics*, vol. 16, no. 2, 2020, Art. no. 026007.
[24] J. Yu, S. Chen, Z. Wu, and W. Wang, "On a miniature free-swimming robotic fish with multiple sensors," *Int. J. Adv. Robot. Syst.*, vol. 13, no. 2, 2016, Art. no. 62, doi: 10.5772/62887.
[25] Accessed: Jul. 1, 2021. [Online]. Available: http://www.yinyanmodel.com/En/ProductView.asp?ID=270
[26] D. Korkmaz, Z. H. Akpolat, S. Soygüder, and H. Alli, "Dynamic simulation model of a biomimetic robotic fish with multi-joint propulsion mechanism," *Trans. Inst. Meas. Control*, vol. 37, no. 5, pp. 684–695, 2015.
[27] V. A. Pham, T. T. Nguyen, B. R. Lee, and T. Q. Vo, "Dynamic analysis of a robotic fish propelled by flexible folding pectoral fins," *Robotica*, vol. 38, no. 4, pp. 699–718, 2020.
[28] J. Yu, J. Yuan, Z. Wu, and M. Tan, "Data-driven dynamic modeling for a swimming robotic fish," *IEEE Trans. Ind. Electron.*, vol. 63, no. 9, pp. 5632–5640, Sep. 2016.
[29] K. A. Morgansen, B. I. Triplett, and D. J. Klein, "Geometic methods for modeling and control of free-swimming fin-actuated underwater vehicles," *IEEE Trans. Robot.*, vol. 23, no. 6, pp. 1184–1199, Dec. 2007.
[30] F. El-Hawary, *The Ocean Engineering Handbook*, Boca Raton, FL, USA: CRC, 2000.
[31] M. Aureli, V. Kopman, and M. Porfiri, "Free-locomotion of underwater vehicles actuated by ionic polymer metal composites," *IEEE/ASME Trans. Mechatronics*, vol. 15, no. 4, pp. 603–614, Aug. 2010.
[32] J. Yuan, J. Yu, Z. Wu, and M. Tan, "Precise planar motion measurement of a swimming multi-joint robotic fish," *Sci. China Inf. Sci.*, vol. 59, no. 9, 2016, Art. no. 92208.
[33] J. Yu, Z. Su, M. Wang, M. Tan, and J. Zhang, "Control of yaw and pitch maneuvers of a multilink dolphin robot," *IEEE Trans. Robot.*, vol. 28, no. 2, pp. 318–329, Apr. 2012.
[34] S. Zhang, Y. Qian, P. Liao, F. Qin, and J. Yang, "Design and control of an agile robotic fish with integrative biomimetic mechanisms," *IEEE/ASME Trans. Mechatronics*, vol. 21, no. 4, pp. 1846–1857, Aug. 2016.

Di Chen received the B.E. degree in automation from Yanshan University, Qinhuangdao, China, in 2015, and the M.E. degree in control science and engineering from Tongji University, Shanghai, China, in 2018. He is currently working toward the Ph.D. degree in computer applied technology with the Institute of Automation, Chinese Academy of Sciences, Beijing, China.

His current research interests include bioinspired underwater robots and aquatic–aerial unmanned vehicles.

Zhengxing Wu received the B.E. degree in logistics engineering from the School of Control Science and Engineering, Shandong University, Jinan, China, in 2008 and the Ph.D. degree in control theory and control engineering from the Institute of Automation, Chinese Academy of Sciences (IACAS), Beijing, China, in 2015.

He is currently an Associate Professor with the State Key Laboratory of Management and Control for Complex Systems, IACAS. His research interests include fast maneuvers of bioinspired robotic fish and gliding motions of robotic dolphins.

Yan Meng received the B.E. degree in mechanical engineering from the School of Mechanical Engineering, University of Science and Technology Beijing, Beijing, China, in 2017. He is currently working toward the Ph.D. degree in control theory and control engineering with the Institute of Automation, Chinese Academy of Sciences, Beijing.

His current research interests include robotic fish and intelligent control systems.

Min Tan received the B.Sc. degree from Tsinghua University, Beijing, China, in 1986, and the Ph.D. degree from the Institute of Automation, Chinese Academy of Sciences (IACAS), Beijing, China, in 1990, both in control science and engineering.

He is currently a Professor with the State Key Laboratory of Management and Control for Complex Systems, IACAS. He has authored or coauthored more than 200 papers in journals, books, and conference proceedings. His research interests include robotics and intelligent control systems.

Junzhi Yu (Fellow, IEEE) received the B.E. degree in safety engineering and the M.E. degree in precision instruments and mechanology from the North University of China, Taiyuan, China, in 1998 and 2001, respectively, and the Ph.D. degree in control theory and control engineering from the Institute of Automation, Chinese Academy of Sciences, Beijing, China, in 2003.

From 2004 to 2006, he was a Postdoctoral Research Fellow with the Center for Systems and Control, Peking University, Beijing. He was an Associate Professor and a Full Professor with the Institute of Automation, Chinese Academy of Sciences, in 2006 and 2012, respectively. In 2018, he joined the College of Engineering, Peking University, as a Tenured Full Professor. His current research interests include intelligent robots, motion control, and intelligent mechatronic systems.